

NASA TM X-579

Classified by authority of NASA

Classification Change Notices No. 113

6/7 2/67

NASA

TECHNICAL MEMORANDUM

X-579

EFFECTIVENESS OF SEVERAL CONTROL ARRANGEMENTS
ON A MERCURY-TYPE CAPSULE

By Robert I. Sammonds and Robert R. Dickey

Ames Research Center
Moffett Field, Calif.

FACILITY FORM 602

N 67 - 32136

(ACCESSION NUMBER)

(THRU)

35

(PAGES)

(CODE)

TMX-579

(NASA CR OR TMX OR AD NUMBER)

31

(CATEGORY)

This material contains information affecting the national defense of the United States within the meaning of the espionage laws, Title 18, U.S.C., Sec. 793 and 794, and the transmission or the revelation of its contents in any manner to an unauthorized person is prohibited by law.

NATIONAL AERONAUTICS AND SPACE ADMINISTRATION

WASHINGTON

October 1961

CONFIDENTIAL

CONFIDENTIAL

NATIONAL AERONAUTICS AND SPACE ADMINISTRATION

TECHNICAL MEMORANDUM X-579

EFFECTIVENESS OF SEVERAL CONTROL ARRANGEMENTS

ON A MERCURY-TYPE CAPSULE*

By Robert I. Sammonds and Robert R. Dickey

SUMMARY

An investigation has been conducted to determine the trim effectiveness of three types of aerodynamic controls (flaps) on a Mercury-type capsule and their effect on the static and dynamic stability of the model. The flap types investigated consisted of (1) an outward extension of the spherical surface of the front face beyond the surface of the cone (spherical flap), (2) a forward extension of the conical surface of the afterbody ahead of the spherical front face (conical flap), and (3) a flat surface perpendicular to the longitudinal axis of the capsule at the juncture of the spherical front face and the conical afterbody (flat flap). Tests were made in a wind tunnel at a Mach number of 3.3 and a Reynolds number of 1.25, based on the maximum diameter of the capsule, and in free flight at a Mach number of 5.5 and a Reynolds number of 0.1 million.

Results of these investigations showed that the conical-type flap had the greatest effectiveness. A flap area equal to approximately 6-1/2 percent of the capsule frontal area would trim the capsule at an angle of attack of -29° , resulting in a lift-drag ratio of approximately 0.45. The spherical flap was the least effective, contributing a moment increment only one-third as great as the conical flap.

The addition of the flaps to the basic model increased the drag but did not appreciably affect either the lift-drag ratio, lift-curve slope, or the static stability. For all the configurations tested, the capsule had a negative lift-curve slope and was statically stable. The model generally remained dynamically unstable with the addition of flaps; however, with certain sizes of the conical flap the model was dynamically stable.

*Title, Unclassified

CONFIDENTIAL
03:12:00:00

INTRODUCTION

The use of lift on a vehicle entering the earth's atmosphere from space-flight missions increases the depth of the permissible entry corridor and also permits the vehicle to maneuver in the atmosphere toward a desired landing point. Trajectory analyses (e.g., refs. 1 and 2) indicate that only a modest lift-drag ratio is necessary to produce beneficial effects. Capsule configurations, such as the Mercury capsule, for example, can generate high enough lift-drag ratios to realize a substantial gain in the entry corridor depth and a useful degree of control over landing point.

Capsule configurations can, in principle, be trimmed at lifting attitudes by offsetting the center of gravity or by the use of reaction or aerodynamic controls. In reference 3, the use of center-of-gravity offset was investigated as a means of trimming a Mercury-type capsule to the desired attitudes. In the present report, a study is presented of aerodynamic controls (flaps attached to the corner of the front face) for the same configuration.

The model investigated had a spherical segment front face, with a radius equal to the frontal diameter, and a conical afterbody of 26.5° half angle. This afterbody was chosen so that at the lifting attitudes of interest, the afterbody would not be exposed to large pressure forces or large heating rates. Several different flap geometries were investigated.

The tests were conducted in the Ames 1- by 3-Foot Supersonic Wind Tunnel No. 1 at a Mach number of 3.3, and in the Ames Pressurized Ballistic Range at a Mach number of 5.5. The Reynolds numbers, based on the maximum face diameter, were 1.25 and 0.1 million, respectively. The results obtained are compared with available simple theories to see if flap effectiveness is predictable.

NOTATION

General

A_f area of flap, sq ft

C_D drag coefficient, $\frac{\text{drag}}{q_\infty S}$

C_p pressure coefficient, $\frac{p_l - p_\infty}{q_\infty}$

CONFIDENTIAL

A
5
0
0

CONFIDENTIAL
DECLASSIFIED

3

d reference diameter (diameter of front face), ft

l length of flap extension, ft

M free-stream Mach number

p static pressure, lb/sq ft

q dynamic pressure, lb/sq ft

R radius of curvature of spherical front face, ft

S reference area, $\frac{\pi d^2}{4}$, sq ft

x, y, z earth-fixed system of axis; also displacements along these axes, ft

α_{trim} angle of attack for $C_m = 0$, deg

δ angle between the tangent to the local surface of the body and the free-stream direction, deg

θ angle subtended by the edges of the flap in a plane normal to the longitudinal axis of the capsule, deg

ρ air density, slugs/cu ft

Ω cone half angle, deg

Wind Tunnel

C_L lift coefficient, $\frac{\text{lift}}{q_\infty S}$

C_m pitching-moment coefficient, $\frac{\text{pitching moment}}{q_\infty S d}$

$\frac{L}{D}$ lift-drag ratio

α angle of attack (angle between the longitudinal axis of the capsule and the free-stream direction), deg

[REDACTED]

CONFIDENTIAL

Free Flight

$C_{L\alpha}$	lift-curve slope, per radian
$C_{m\alpha}$	restoring-moment-curve slope (equivalent to pitching-moment-curve slope used in the wind tunnel), $-\frac{8\pi^2 I_y}{\lambda^2 \rho S d}$, per radian
$C_{mq} + C_{m\dot{\alpha}}$	damping-in-pitch derivative, sec^{-1}
I_y	average transverse moment of inertia, slug-ft ²
α	angle of attack (angle between the longitudinal axis of the capsule and the free-stream direction projected onto the x, z plane), deg
α_r	resultant angle of attack, $\sqrt{\alpha^2 + \beta^2}$, deg
α_{RMS}	root-mean-square resultant angle of attack, $\sqrt{\frac{\int_0^x \alpha_r^2 dx}{x}}$, deg
β	angle of sideslip (angle between longitudinal axis of the capsule and the free-stream direction projected onto the x, y plane), deg
λ	wave length of pitching oscillation with respect to the air stream, $\frac{2\pi}{\sqrt{\omega_1 \omega_2}}$, ft
ξ	dynamic stability parameter, $C_D - C_{L\alpha} + (C_{mq} + C_{m\dot{\alpha}}) \left(\frac{d}{\sigma}\right)^2$
σ	transverse radius of gyration, $\frac{I_y}{d^2}$, ft
ω_1, ω_2	rates of rotation of complex vectors which generate the model pitching motion (see ref. 6), radians/ft
$(\dot{})$	first derivative with respect to time

~~CONFIDENTIAL~~
~~DECLASSIFIED~~

5

Subscripts

- ∞ free-stream condition
- λ local condition after bow shock

MODELS


The basic configuration tested was a body of revolution consisting of a 26.5° half-angle conical afterbody and a spherical segment front face, having a face diameter to radius-of-curvature ratio (d/R) equal to 1. The cone half angle of 26.5° was selected in accordance with the considerations presented in the Introduction and in reference 3.

Three types of aerodynamic controls, shown in the sketches of figure 1, were investigated in conjunction with the basic model: (1) an outward extension of the spherical surface beyond the cone, (2) a forward extension of the conical surface ahead of the spherical front face, and (3) a flat surface perpendicular to the longitudinal axis of the capsule at the juncture of the spherical front face and the conical afterbody. These three flap configurations are hereinafter referred to as the "spherical," "conical," and "flat" flaps, respectively. As shown in figure 1(a), the wind-tunnel models consisted of three different sized spherical flaps and one each of the conical- and flat-type flaps. The free-flight models, as shown in figure 1(b), consisted of four different sized spherical flaps and four different sized conical flaps. Photographs of the flap installation on the wind-tunnel and free-flight models are shown in figures 2 and 3, respectively. The variation of the flap area with θ and λ is presented in figure 4.

The wind-tunnel models had a portion of their afterbodies removed to facilitate mounting them on the tunnel support system. The models tested in free flight were of homogeneous construction, having their centers of gravity located at 0.33 of the maximum diameter aft of the front face. This location was taken to be the moment center for all of the free-flight and wind-tunnel tests.

TESTS AND REDUCTION OF DATA

The procedures used and the accuracies obtained for each facility will be briefly described.



CONFIDENTIAL

Wind-Tunnel Tests

The lift, drag, and pitching moment of the models were measured at angles of attack from $+30^\circ$ to -45° by means of a flexure-type strain-gage balance. The balance extended rearward from the base of the model and was shielded from the air stream by a $7/8$ -inch-diameter shroud.

The effects of wall interference, tunnel stream angle, and pressure gradients are believed to be negligible for these tests. The base drag correction arising from the difference between the free-stream static pressure and the static pressure measured at the cut-off base of the model was found to be small and is not included in the coefficients presented in this report.

The mean square values of the random errors of measurement, evaluated by the method of reference 4, are given in the following table:

M	± 0.02
α	$\pm 0.10^\circ$
C_L	± 0.010
C_D	± 0.016
C_m	± 0.012
L/D	± 0.010

A
5
0
0

Pressurized-Ballistic-Range Tests

Models were launched in free flight from a caliber 50 powder gas gun at initial muzzle velocities of approximately 6300 feet per second. The models were adapted to the gun by means of a two-piece plastic (Lexan) sabot which launched the model at nearly its design trim angle. Photographs of two of the flapped models and their 20° canted sabots are shown in figure 3.

Shadowgraph pictures, triggered by the model, were obtained in 2 orthogonal planes at 17 observation stations, for a ballistic flight of 130 feet. The photographic observation stations are calibrated and referenced in such a manner that the spatial position and the attitude of the model at each station may be determined with respect to an orthogonal system of axes for the entire range. An electronic chronograph was used to measure the time of flight between stations. The accuracies involved in determining the model position, orientation, and time of flight are as follows:

x, y, z	± 0.005 inch
α, β	$\pm 0.1^\circ$

[REDACTED]

CONFIDENTIAL

7

A
5
0
0

The reduction of the trajectory data to force and moment coefficients was accomplished by the method described in reference 5. By this method the best suited aerodynamic coefficients and initial conditions are selected by an iterative process to fit the equations of motion to the particular motion under consideration. In the present case, the equations of motion given in reference 6 were used to obtain the stability coefficients and lift-curve slope (including the effects of trim and roll). For the flapped models of this investigation, the reduction of the trajectory data to force and moment coefficients on the basis of these formulas is complicated by the fact that the models are not axially symmetric and were trimmed to fly at angle of attack. However, it has been shown in reference 6 that the equations of motion are applicable to models with small amounts of asymmetry and relatively low amplitudes of oscillation and that they can be solved for both roll rate and trim angle. The degree to which the iterative process converges in fitting these equations of motion to the experimental data is indicative of the accuracy with which the experimental data can be matched. Motions having large oscillation amplitudes (greater than about $\pm 20^\circ$) and/or large trim angles (greater asymmetry) either did not converge at all or did not converge to a reasonable degree of accuracy so that it was not possible to analyze these runs by the above method. However, the trim angle of attack can be determined from the positions of the tricyclic vectors (ref. 6) on a plot of α versus β .

In addition, runs in which the model has negligible roll and does not precess (see ref. 6) can be analyzed to determine trim angle and static stability by fitting the motions of the model to sine waves. This method of analysis, like the more general method of reference 6, assumes that the model has linear aerodynamic moment coefficients. For the data presented herein, the machine fit to α and β resulted in RMS errors of less than $\pm 1.5^\circ$ for all cases except that the error was $\pm 2.5^\circ$ with the 90° conical flap ($\alpha_{\text{trim}} = -15^\circ$).

The drag coefficients presented herein for the free-flight models were reduced basically by the method of reference 7, which was modified to allow for variations of the drag coefficient with angle of attack.

A procedure applicable to cases where the drag coefficient varies with the angle of attack squared is presented in reference 8. For the present investigation, the assumed variation of drag coefficient with resultant angle of attack was modified by the addition of a fourth-power term as described in reference 3. However, it can still be shown, in a manner similar to that used in reference 8, that the effective constant drag coefficient obtained from the present data by the method of reference 7, and under the same constraints, is equivalent to the drag coefficient that would be obtained at a constant angular displacement equal to the root-mean-square angle of attack, averaged over the distance interval of the trajectory.

[REDACTED]

CONFIDENTIAL
03:12:28:1934

RESULTS AND DISCUSSION

Wind-Tunnel Tests

Force and moment data obtained from the wind-tunnel tests are presented in figures 5 through 8 as a function of angle of attack.

Basic capsule.- Figure 5 shows a comparison of the measured values of C_L , C_D , C_m , and L/D for the basic capsule with those predicted by modified Newtonian impact theory ($C_p = 1.76 \sin^2 \delta$). Two theoretical curves are presented for angles of attack greater than $26\frac{1}{2}^\circ$ - one based on the front face alone and the other including the effect of the afterbody. In general, agreement between theory and experiment is quite good, especially at angles of attack up to $\pm 25^\circ$. Above 25° , better agreement between theory and experiment is obtained where the effect of the afterbody is included in the theory. It can be noted that the capsule develops lift-drag ratios above 0.5 in the angle range above 35° , at lift coefficients between 0.4 and 0.5; $C_{m\alpha}$ becomes rather small and possibly negative above 40° angle of attack.

A
5
0
0

Capsule with the three basic types of flap controls.- Figure 6 presents a comparison of the measured values of C_L , C_D , C_m , and L/D for the basic capsule and for the three different flapped configurations (spherical, conical, and flat) having equivalent sized flaps ($l/d = 0.09$, $\theta = 45^\circ$, $A_f/S = 0.049$). For all flap types, the capsule was statically stable at trim attitude. The conical type was the most effective for a given flap area; that is, it trimmed the capsule ($C_m = 0$) at the highest negative angle of attack and thus developed the highest trimmed lift-drag ratio, 0.42 at trim. The nearly linear variation of the lift-drag ratio with angle of attack obtained for these configurations indicates that trim angles in excess of 30° will be required to produce lift-drag ratios of the order of 0.5 for this face curvature. (See ref. 3 for a discussion of the effect of face curvature on L/D .)

Figure 7 presents a comparison of the measured values of C_L , C_D , C_m , and L/D for three different sized spherical flaps ($A_f/S = 0.049$, 0.067, 0.098).

ΔC_m .- Incremental values of pitching-moment coefficient for the three types of flaps, obtained by subtracting the pitching moment of the basic model from the total pitching moment of the model with flaps, are presented in figure 8. These data clearly show the superiority of the conical flap at the higher negative angles of attack. Incremental pitching moments predicted for the flaps by modified Newtonian impact theory, shown by the dashed lines, are in error for the conical flaps because a stagnation point in the flow can be expected to occur on the windward surface of these flaps. Although it is not entirely logical to assume that the stagnation pressure occurs over the entire windward

[REDACTED]

DECLASSIFIED

surface of the flap because of end effects, etc., this assumption appears to give a good first approximation for predicting the effect of the flap. On this basis, equation (A1) was used to predict incremental values of pitching moment due to the flap. The predicted values of ΔC_m , presented in figure 8, show better agreement with the experimental results than those predicted by impact theory, although this method still underestimates the flap effectiveness at negative angles of attack. At high negative angles of attack ($\alpha < -20^\circ$ for these test conditions), a secondary shock associated with the flap reduces the flap effectiveness; equations (A2) were used to predict incremental values of pitching moment and reasonable agreement was obtained with the experimental data.

Free-Flight Tests

Force, trim, and static and dynamic stability data derived from free-flight tests of the basic model (ref. 3) and of two of the flapped configurations (spherical and conical) are presented in figures 9 through 13.

Trim effectiveness.— The data presented in figure 9 show the trim effectiveness of various sized flaps of both the spherical and conical types. These data show that the flap effectiveness is directly a function of the flap area and type and is not particularly a function of either θ or l , except insofar as they are effective in changing the flap area. A conical-type flap having an area ratio (A_f/S) of 0.06 would trim the capsule at approximately $26-1/2^\circ$, which is better than three times as effective as a spherical flap of comparable size.

In the case of the spherical flap, figure 9(a), it can be seen that the experimental data obtained in free flight agree well with that predicted by modified Newtonian impact theory ($C_{p_t} = 1.8$, appropriate to the test Mach number). Included in figure 9(a) are experimental values of α_{trim} obtained from the wind-tunnel tests (fig. 7). These data agree within the experimental uncertainty (indicated by horizontal length of the bars) with impact theory and with the free-flight results.

In the case of the conical flap, figure 9(b), agreement of the experimental data with impact theory is poor, as noted earlier. However, theoretical values of trim angle of attack, predicted by equations (A1) and (A2) of the appendix, show reasonable correlation with the free-flight data. Comparison of the free-flight data with that obtained in the wind tunnel shows that the wind-tunnel test gave a considerably higher trim angle of attack. It is felt that this lack of agreement is due to afterbody effects resulting from the fact that the wind-tunnel models had a portion of their afterbodies removed to accommodate the model support system.

CONFIDENTIAL

CONFIDENTIAL

1. The trim effectiveness of the conical flap was superior to that of the flat and spherical types, resulting in a trim angle of attack of approximately -29° for a flap size equal to 6.3 percent of the capsule frontal area. For the spherical flap, however, the same size flap resulted in a trim angle of attack of only -9° .

2. For a given angle of attack, the effect of the size and shape of the flap on the lift-drag ratio was small. Extrapolation of these data shows that at trim angles of attack, around 35° , lift-drag ratios of the order of 0.5 are obtained.

3. The static stability of the basic configuration was not greatly affected by the addition of flaps. However, the conical-type flaps were slightly destabilizing, whereas the spherical type were slightly stabilizing. In all cases, the capsule was statically stable at the trim angle of attack.

A
5
0
0

4. The dynamic stability of the basic configuration was increased by the addition of the 45° conical flap but was relatively unaffected by either the spherical or 90° conical flaps. In all cases, the 45° conically flapped models were dynamically stable, whereas the spherically and 90° conically flapped models were generally dynamically unstable.

5. Modified Newtonian impact theory predicted quite well the effectiveness of the spherical flap and reasonably well the effectiveness of flat-type flaps, but badly underestimated the effectiveness of the conical flap. However, on the assumption that stagnation pressure acts on the flap face, it is possible to predict the characteristics of the conical flap.

Ames Research Center

National Aeronautics and Space Administration
Moffett Field, Calif., Aug. 11, 1961



APPENDIX A

FORMULAS FOR PREDICTING THE FLAP EFFECTIVENESS OF THE CONICAL-TYPE FLAP

If the windward side of the flap is assumed to be at stagnation pressure, the effectiveness of the conical-type flap is

$$\Delta C_{mf} = - \frac{2C_{pt}}{SR} \int_0^{\theta/2} \int_{r_1}^{r_2} \left[\frac{r^2 \cos \theta}{\sin^2 \Omega} - \frac{\bar{C}}{\tan \Omega} (r \cos \theta) \right] dr d\theta \quad (A1)$$

where

C_{pt} = total pressure coefficient across a normal shock

$$r_1 = d/2$$

r_2 = the radial distance from the longitudinal center line of the model to the leading edge of the flap, $r_1 + l \sin \Omega$

$$\bar{C} = R \left[\frac{1}{2 \tan \Omega} + (1 + \Delta) - \frac{\sqrt{R^2 - r_1^2}}{R} \right]$$

Δ = center-of-gravity location, in percent of the maximum face diameter, aft of the front face

However, as the angle of attack becomes more negative, a point will be reached at which the local flow over the front face of the model will become supersonic, resulting in a secondary shock wave associated with the flap. When this condition occurs ($M_1 \geq 1.0$), the pressures on the flap can be calculated by means of the embedded Newtonian flow theory of reference 9, specifically by use of the equation

$$C_{pf} = C_{p_l} + 2 \left(\frac{q_1}{q_\infty} \right) \sin^2 \mu = C_{pt} \sin^2 \delta + 2 \left(\frac{q_1}{q_\infty} \right) \sin^2 \mu$$

where μ is the angle between the secondary shock and the surface of the model. For the data presented herein, the secondary shock was assumed to be a normal shock ($\mu = 90^\circ$).

CONFIDENTIAL

Thus, for these conditions ($M_1 \geq 1.0$, as determined by Newtonian concepts) the equation for the flap effectiveness can be given by

$$\Delta C_{m_F} = - \frac{2C_{p_F}}{SR} \int_0^{\theta/2} \int_{r_1}^{r_2} \left[\frac{r^2 \cos \theta}{\sin^2 \Omega} - \frac{\bar{C}}{\tan \Omega} (r \cos \theta) \right] dr d\theta \quad (A2)$$

It is expected that the above equations will tend to underestimate the effectiveness of the flaps because interference of the flap with flow on the model front face has not been accounted for. This interference will produce local regions of increased pressure on the model face and contribute to the total pitching-moment increment attributable to deflection of the flap.

A
5
0
0

CONFIDENTIAL

CONFIDENTIAL
DECLASSIFIED

15

REFERENCES

1. Chapman, Dean R.: An Analysis of the Corridor and Guidance Requirements for Supercircular Entry Into Planetary Atmospheres. NASA TR R-55, 1959.
2. Levy, Lionel L., Jr.: An Approximate Analytical Method for Studying Atmosphere Entry of Vehicles With Modulated Aerodynamic Forces. NASA TN D-319, 1960.
3. Intrieri, Peter F.: Effects of Transverse Center-of-Gravity Displacement, Afterbody Geometry, and Front-Face Curvature on the Aerodynamic Characteristics of Mercury-Type Models at a Mach Number of 5.5 NASA TM X-569, 1961.
4. Beers, Yardley: Introduction to the Theory of Error. Addison-Wesley Publishing Co., Cambridge, Mass., 1953.
5. Sommer, Simon C., Short, Barbara J., and Compton, Dale L.: Free-Flight Measurements of Static and Dynamic Stability of Models of the Project Mercury Re-entry Capsule at Mach Numbers 3 and 9.5. NASA TM X-373, 1960.
6. Nicolaidis, John D.: On the Free Flight Motion of Missiles Having Slight Configurational Asymmetries. BRL Rep. 858, Aberdeen Proving Ground, 1953 (IAS Preprint 395).
7. Seiff, Alvin: A New Method for Computing Drag Coefficients From Ballistic Range Data. Jour. Aero. Sci., vol. 25, no. 2, Feb. 1958, pp. 133-134.
8. Seiff, Alvin, and Wilkins, Max E.: Experimental Investigation of a Hypersonic Glider Configuration at a Mach Number of 6 and at Full-Scale Reynolds Numbers. NASA TN D-341, 1961.
9. Seiff, Alvin, and Whiting, Ellis E.: The Effect of the Bow Shock Wave on the Stability of Blunt-Nosed Slender Bodies. NASA TM X-377, 1960.

[REDACTED]

CONFIDENTIAL

E

T

A
5
0
0

.

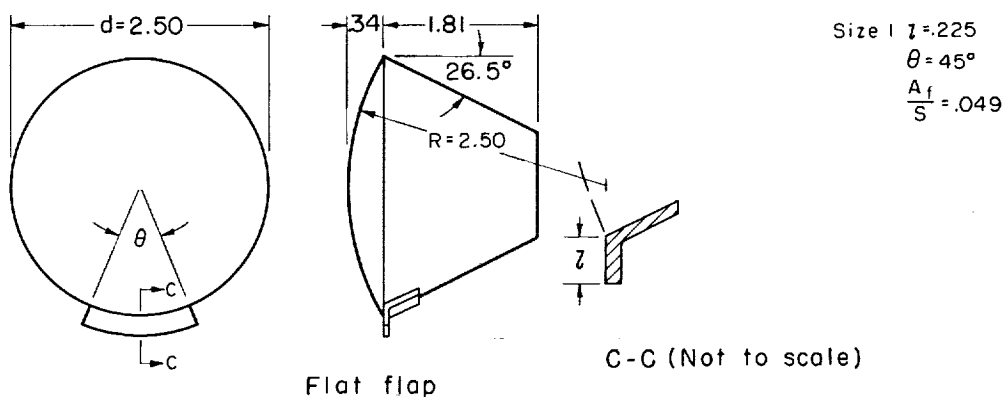
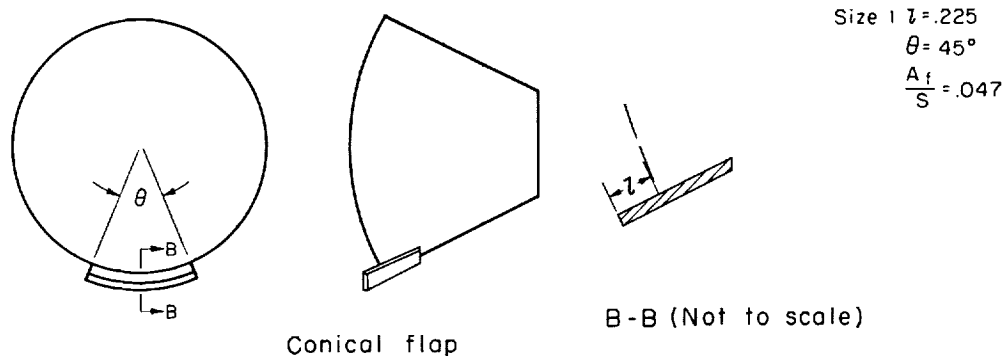
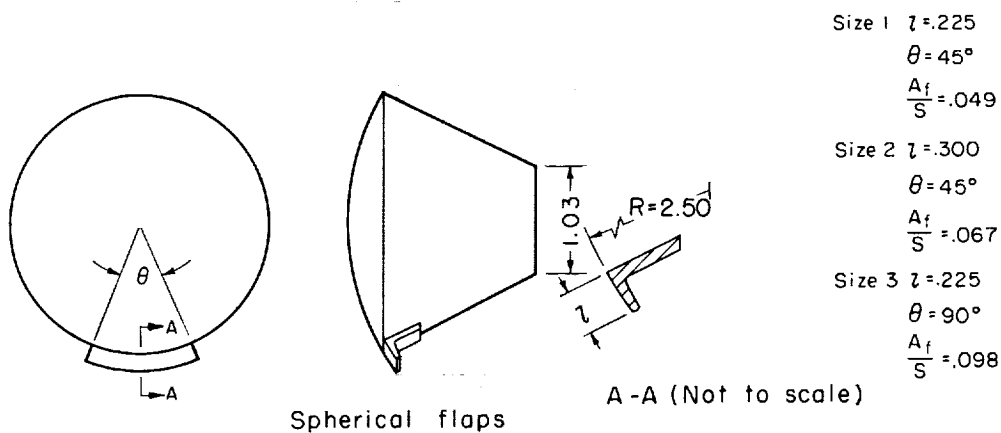
.

T

T

CONFIDENTIAL

CONFIDENTIAL

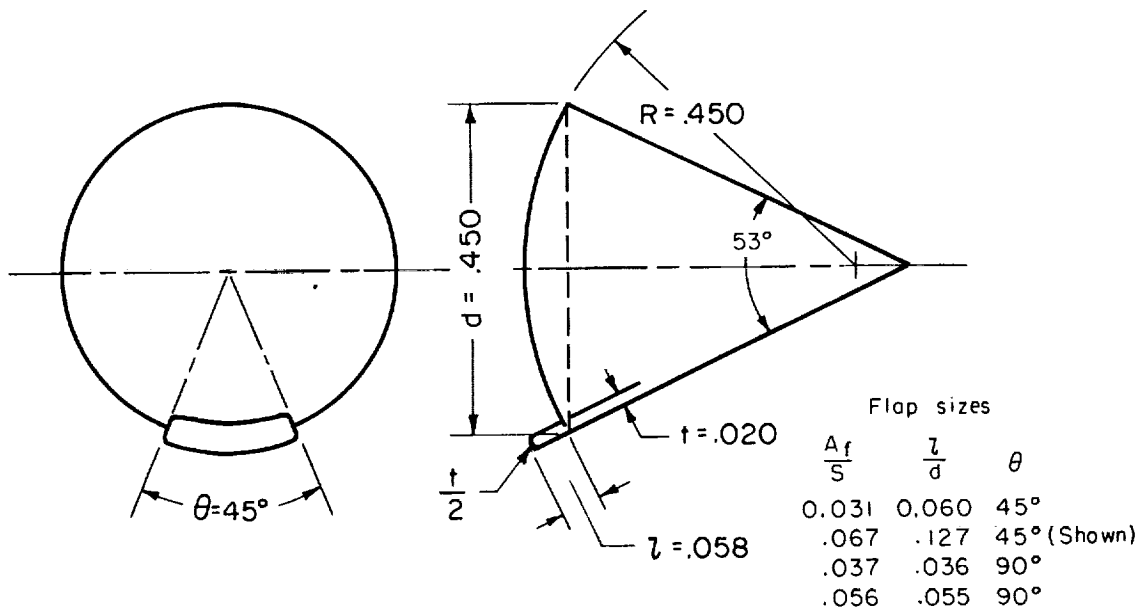
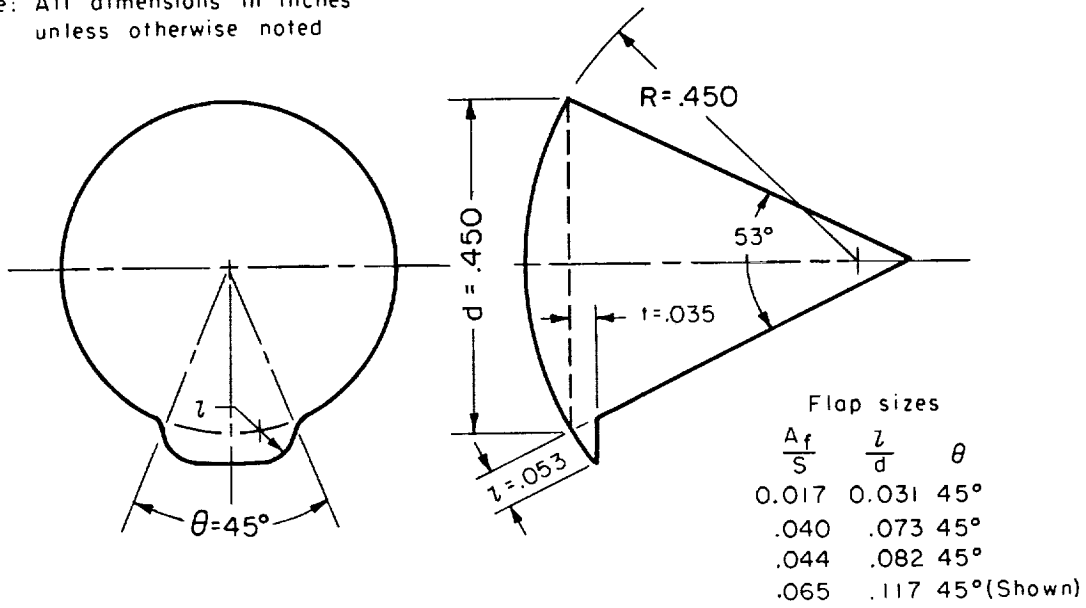


(a) Wind-tunnel models.

Figure 1.- Model arrangement.

CONFIDENTIAL

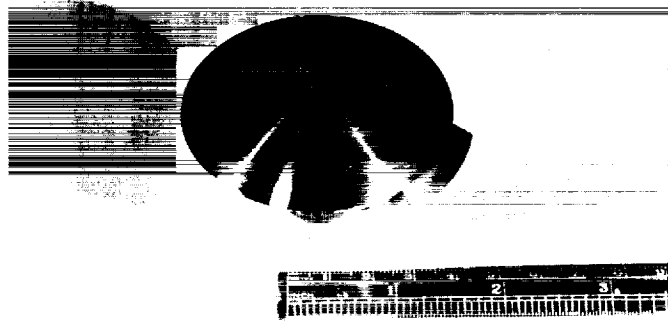
Note: All dimensions in inches
unless otherwise noted



(b) Free-flight models.

Figure 1.- Concluded.

CONFIDENTIAL



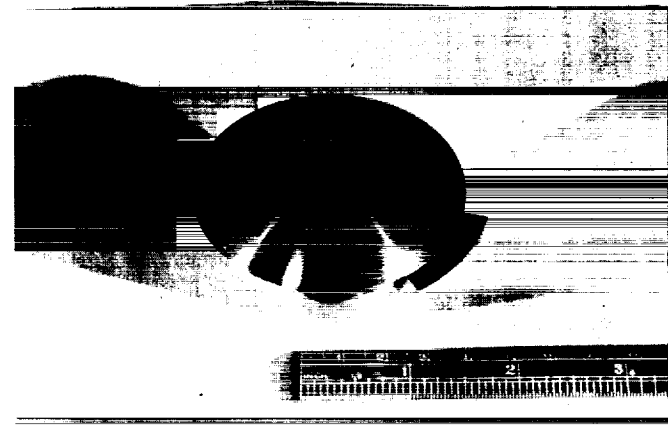
(a) Spherical flap.

A-27370



(b) Conical flap.

A-27372



(c) Flat flap.

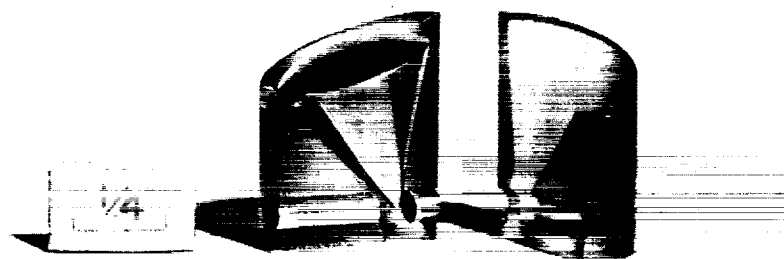
A-27371

Figure 2.- Photographs of wind-tunnel models.



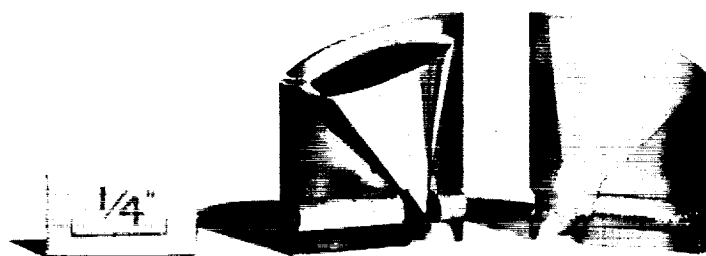
A
5
0
0

CONFIDENTIAL



(a) Spherical flap.

A-28171



(b) Conical flap.

A-28172

Figure 3.- Photographs of free-flight models and sabots.

[REDACTED]

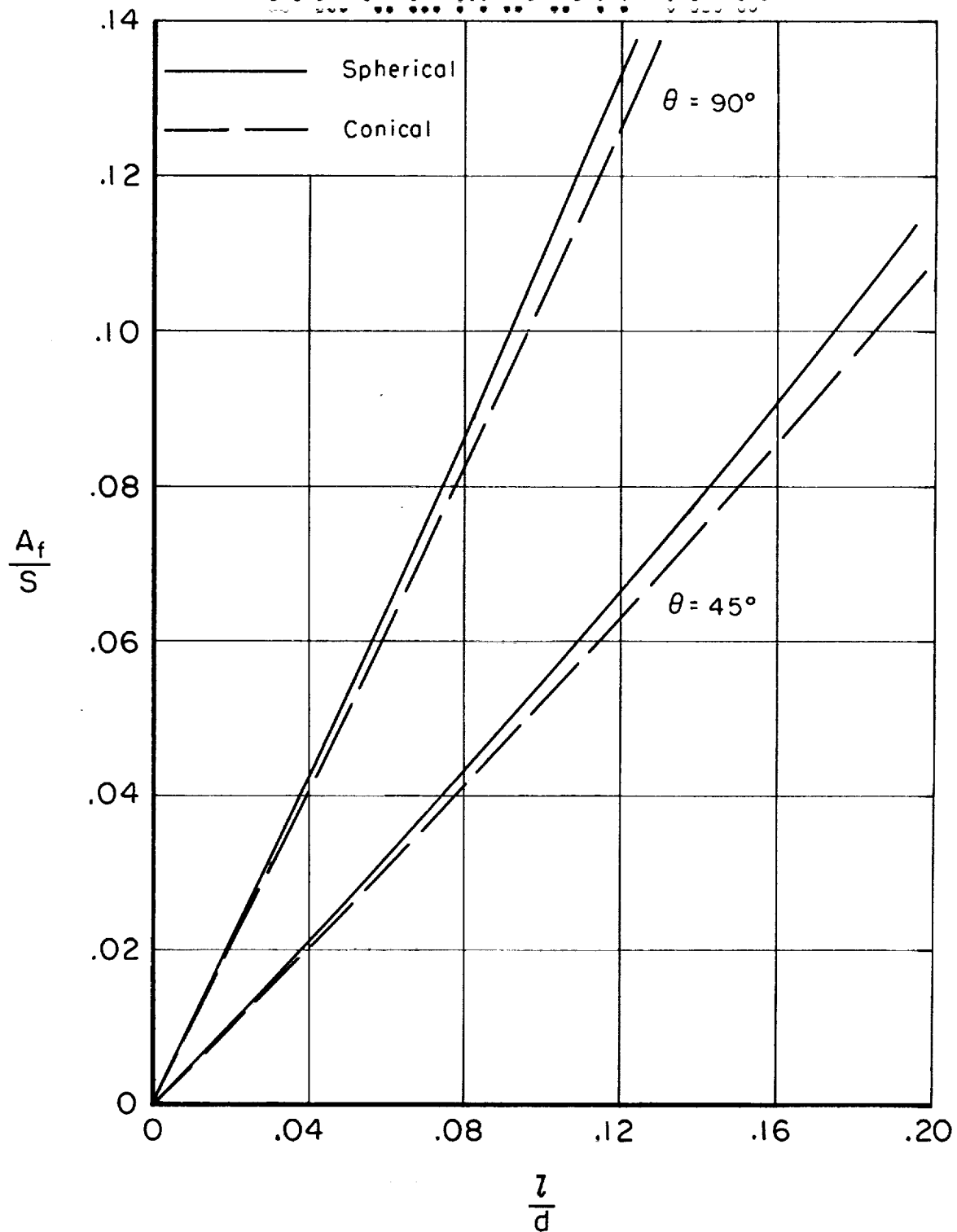


Figure 4.- Variation of flap area with flap extension.

CONFIDENTIAL

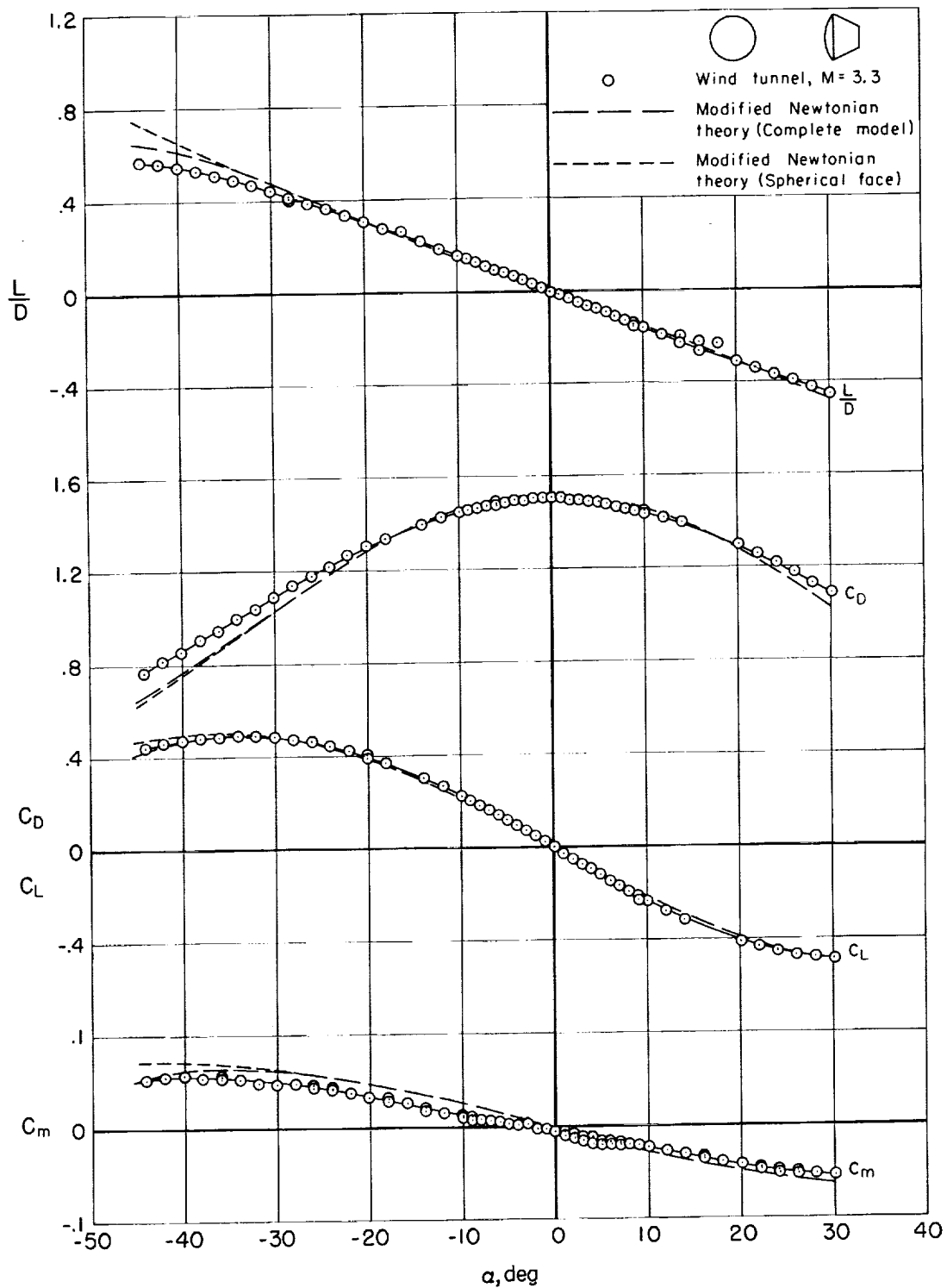


Figure 5.- Aerodynamic characteristics of the basic capsule.

CONFIDENTIAL

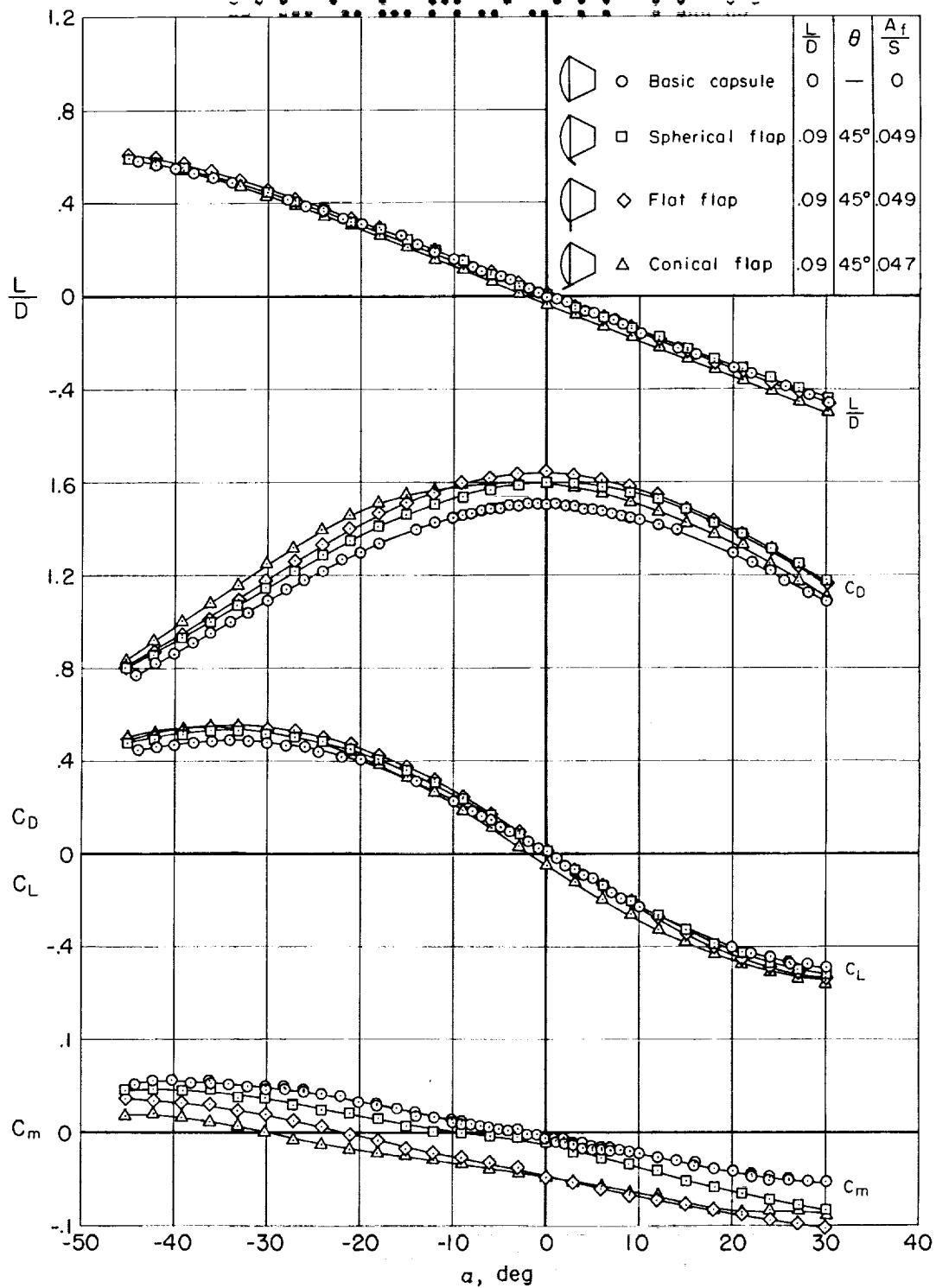


Figure 6.- Effect of flap shape on the aerodynamic characteristics of body-flap combinations.

CONFIDENTIAL

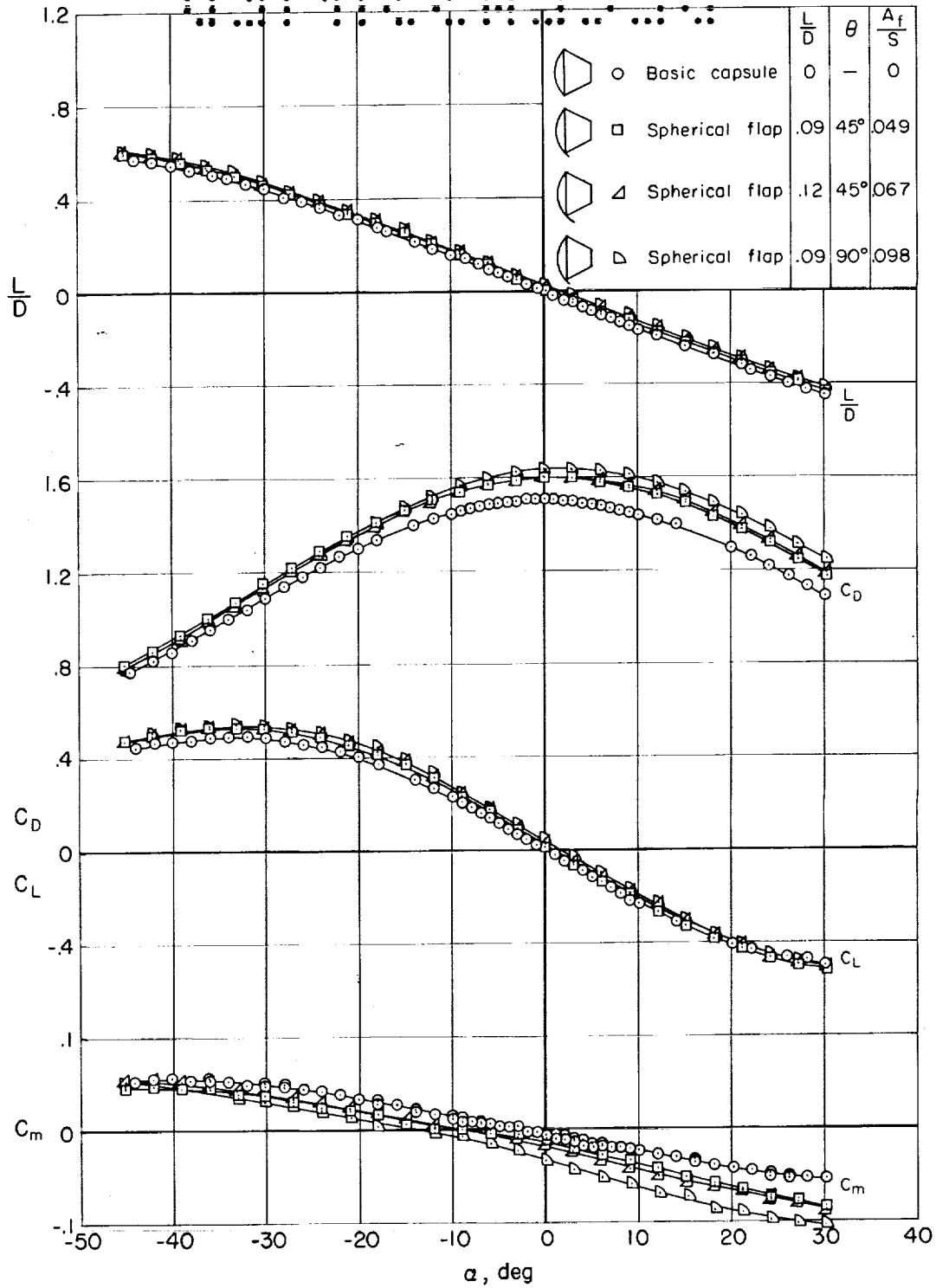


Figure 7.- Effect of flap size on the aerodynamic characteristics of body with a spherical flap.

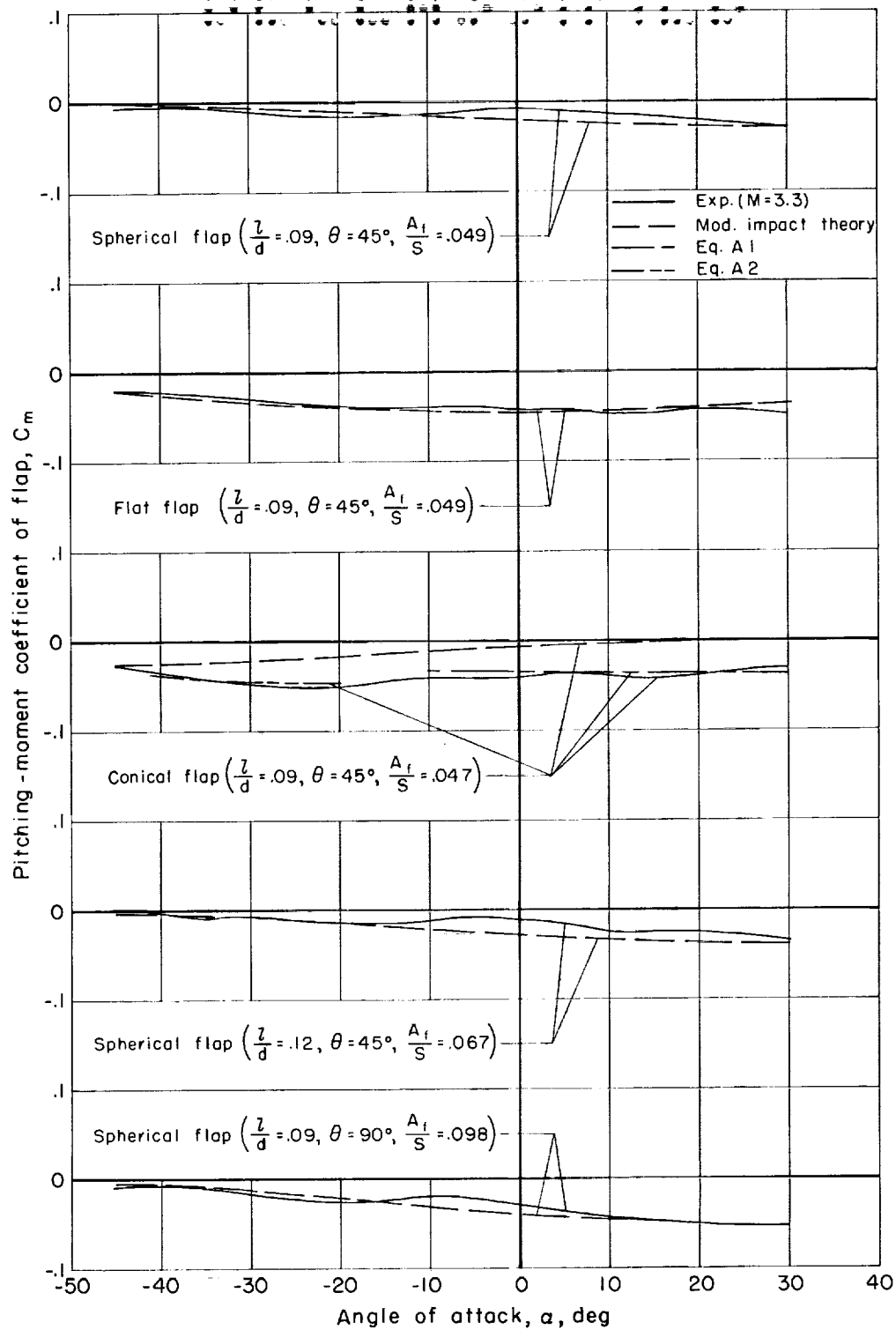
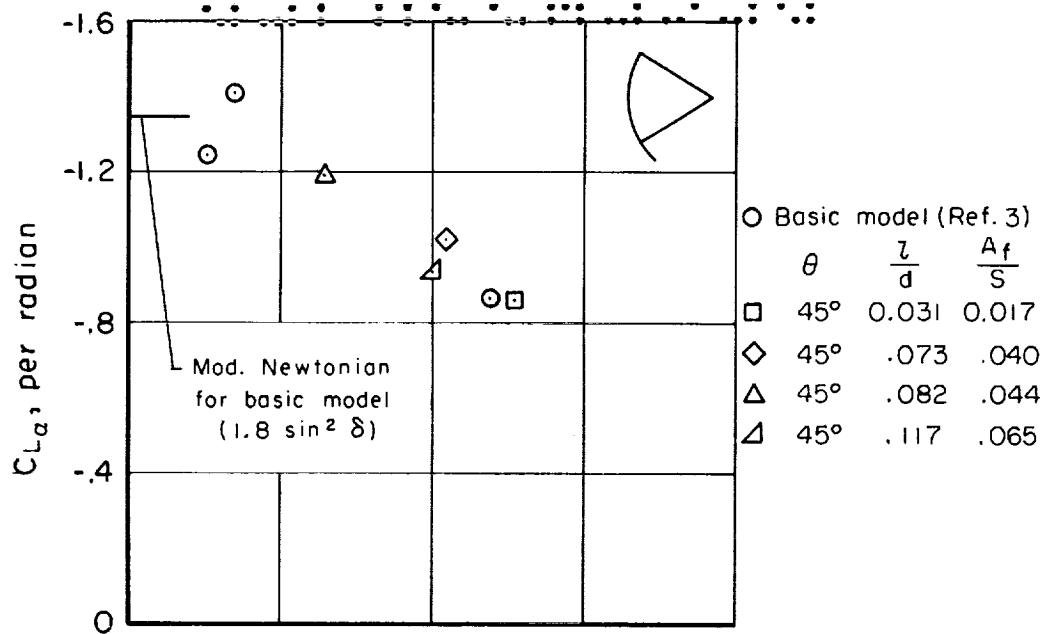
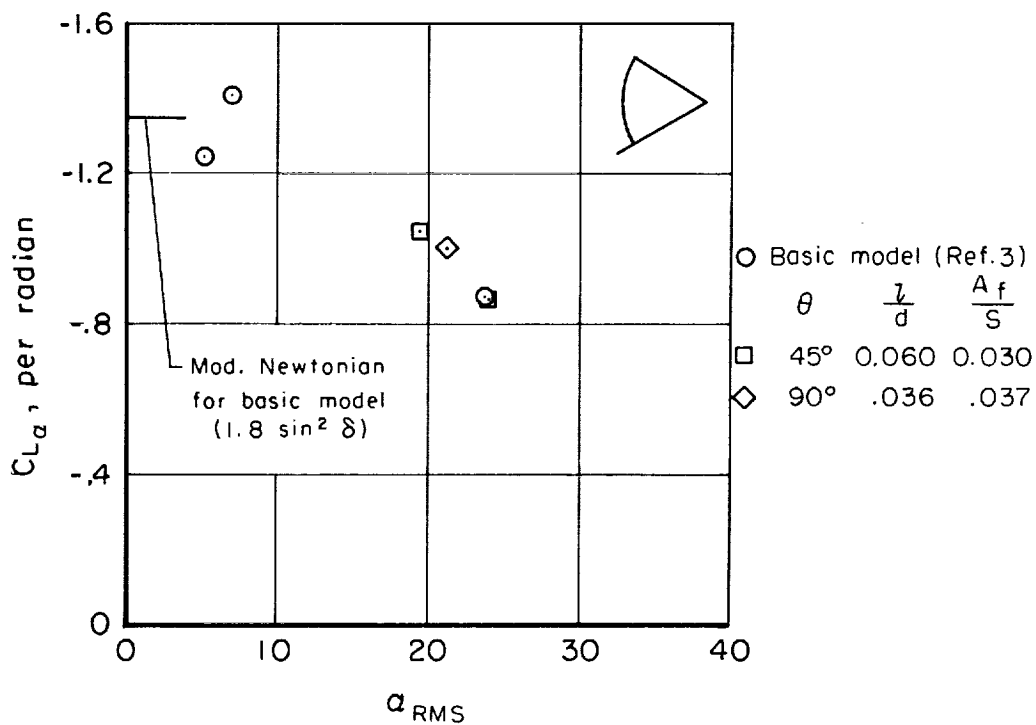


Figure 8.- Pitching-moment coefficients of the flaps.

CONFIDENTIAL

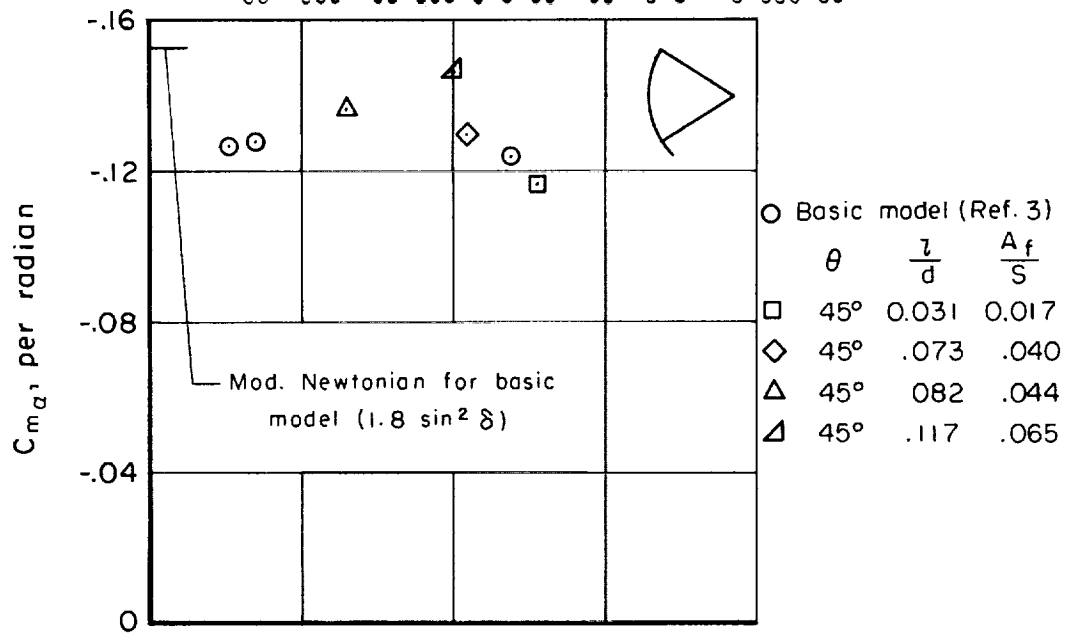


(a) Spherical flap.

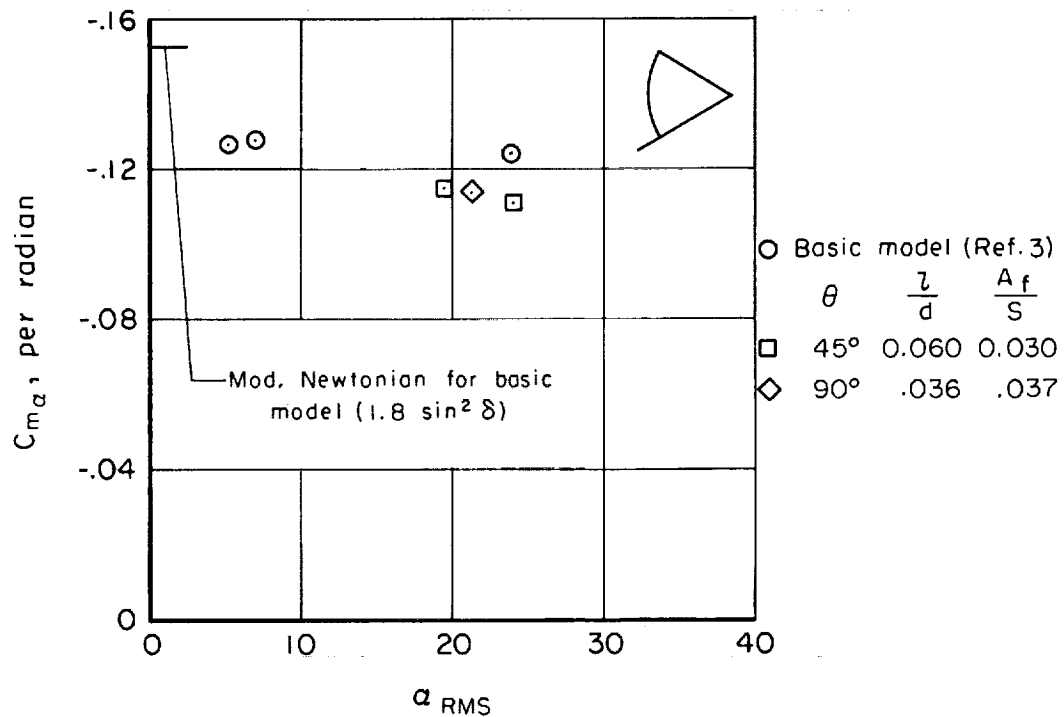


(b) Conical flap.

Figure 11.- Lift-curve slope of free-flight models.



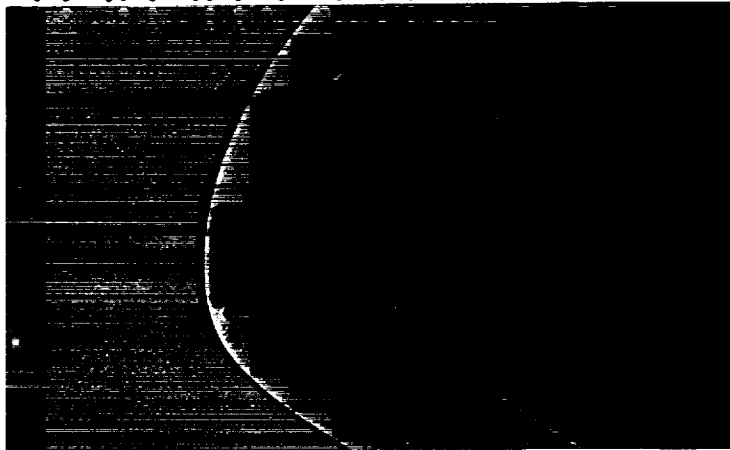
(a) Spherical flap.



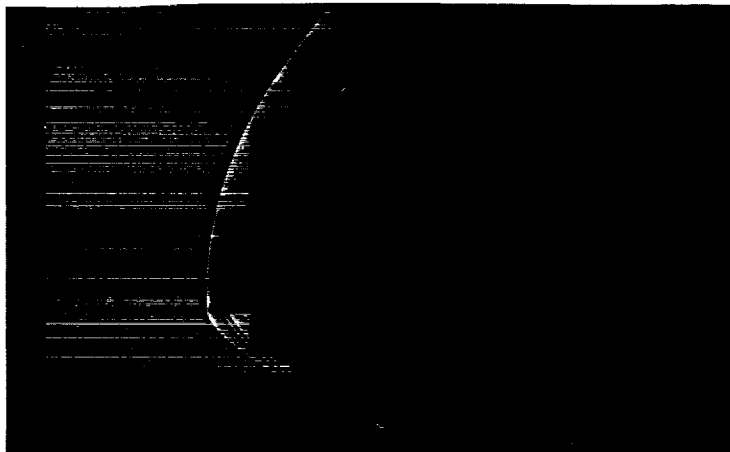
(b) Conical flap.

Figure 12.- Static stability of free-flight models.

CONFIDENTIAL



(a) Spherical flap, $\alpha = 30^\circ$.



(b) Conical flap, $\alpha = 30^\circ$.



(c) Flat flap, $\alpha = 30^\circ$.

Figure 14.- Typical shadowgraph pictures of sting mounted models in the wind tunnel; $M = 3.3$, $R = 1.25 \times 10^6$.

L

A
5
C
C

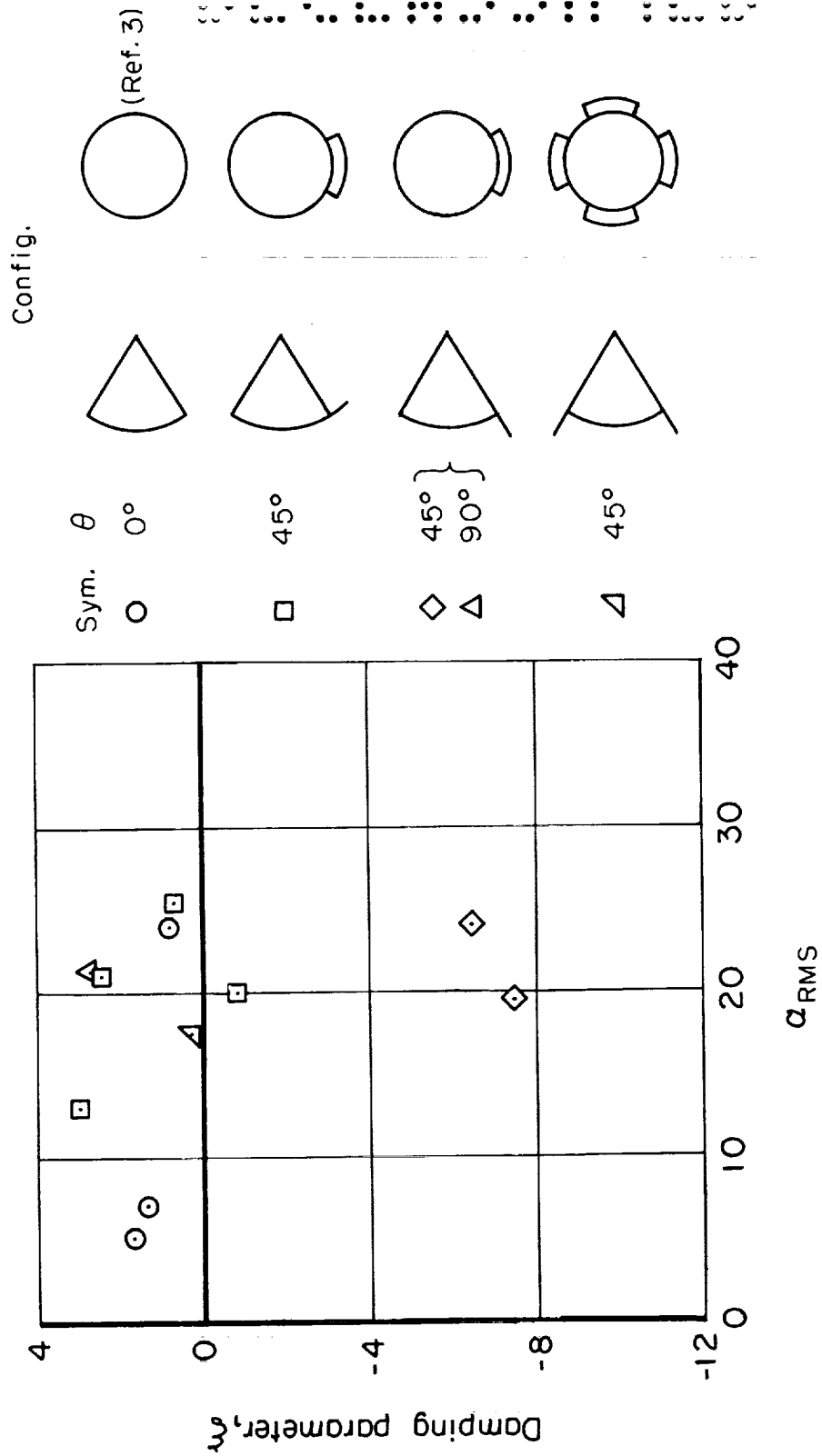


Figure 13.- Dynamic stability of free-flight models.

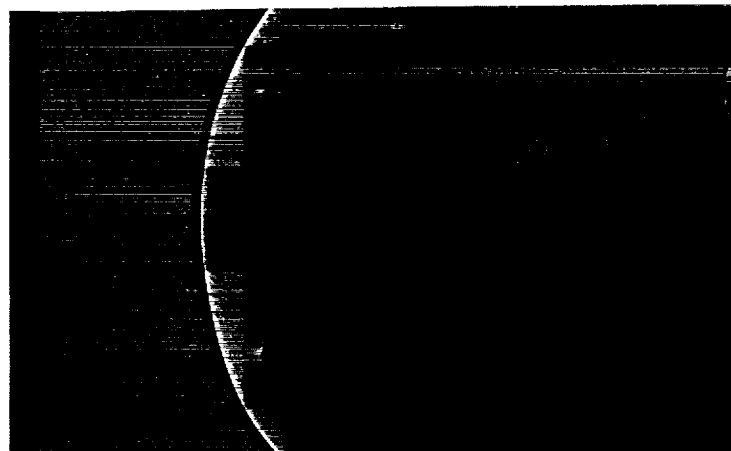
CONFIDENTIAL



(d) Spherical flap, $\alpha = 0^\circ$.



(e) Conical flap, $\alpha = 0^\circ$.

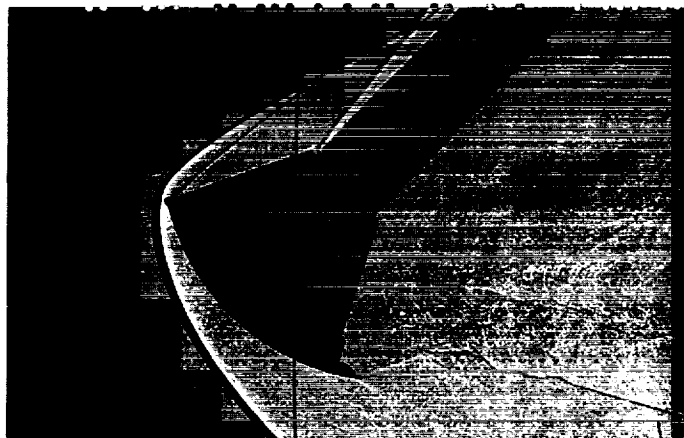


(f) Flat flap, $\alpha = 0^\circ$.

Figure 14.- Continued.

~~CONFIDENTIAL~~

A
5
0
0



(g) Spherical flap, $\alpha = -45^\circ$.



(h) Conical flap, $\alpha = -45^\circ$.

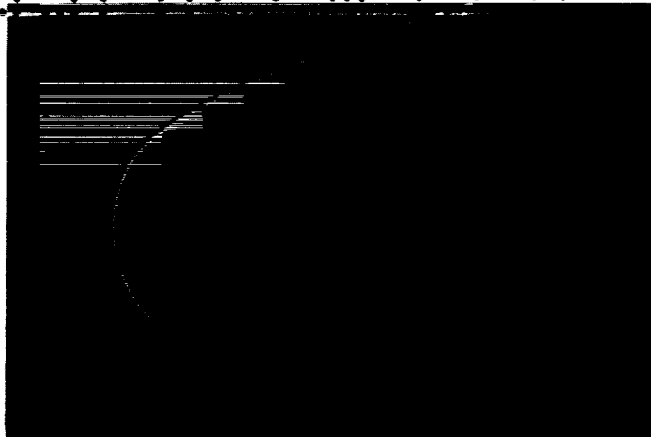


(i) Flat flap, $\alpha = -45^\circ$.

Figure 14.- Concluded.

~~CONFIDENTIAL~~

CONFIDENTIAL



$$\alpha = -1.4^\circ$$



$$\alpha = -14.5^\circ$$



$$\alpha = -45.6^\circ$$

(a) Spherical flap.

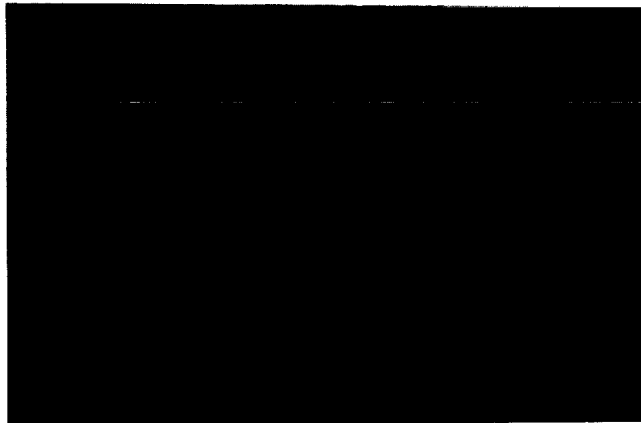
Figure 15.- Typical shadowgraph pictures of models in free flight;
 $M = 5.5$, $R = 0.1 \times 10^6$.

[REDACTED]

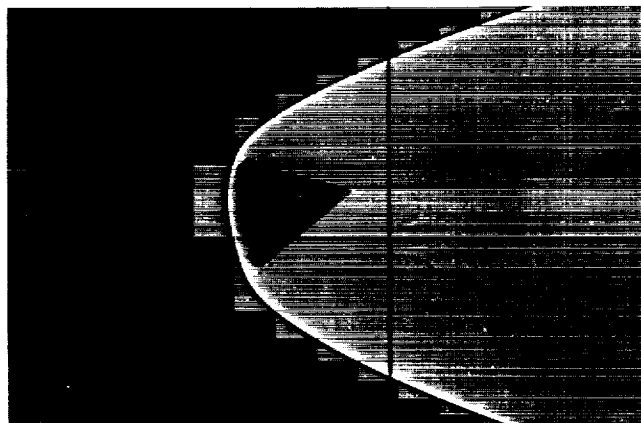
A
5
0
0

CONFIDENTIAL

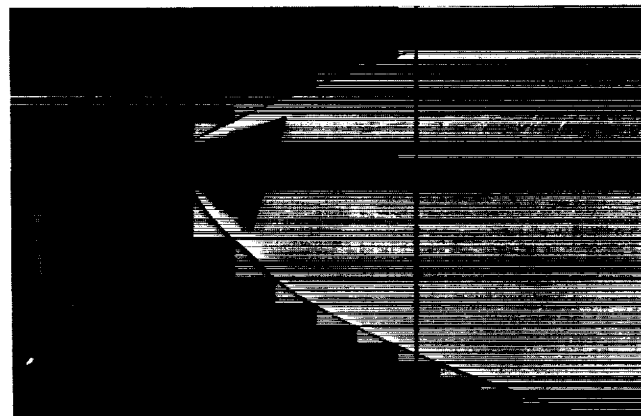
35



$$\alpha = -2.2^{\circ}$$



$$\alpha = -12.2^{\circ}$$



$$\alpha = -49.0^{\circ}$$

(b) Conical flap.

Figure 15.- Concluded.

CONFIDENTIAL

03174229.1030

03174229.1030

03174229.1030

03174229.1030

03174229.1030

03174229.1030

03174229.1030